Journal of Network Intelligence
Taiwan Ubiquitous Information
 ISSN 2414-8105
Volume **9**, Number **1**, February **2024**

Research on Commutator Surface Defect Detection Technology based on Class Neural Network

Yufeng Shu, Changwei Xiong

Intelligent Manufacturing College
Dongguan Polytechnic, Dongguan 523808, China
Guangdong Textile Industry Intelligent Detection Engineering Technology Research Center (DGPT)
Dongguan 523808, China
meyufeng@163.com, 513268403@qq.com

Zhongming Xie*

Shini Plastics Technologies (Dongguan), Inc.
Dongguan 523808, China
Johnny.xie@cn.shini.com

*Corresponding author: Zhongming Xie
Received October 20, 2022, revised January 3, 2023, accepted July 3, 2023.

Abstract. *The technical difficulties of commutator surface defect detection system originate from how to meet the requirements of high efficiency, high accuracy and real-time industrial inspection. The commutator has large curved surface and high reflectivity, and the traditional manual inspection has the disadvantages of time consuming, leakage and error detection. In this study, a commutator surface defect detection method is constructed using spatial domain image processing method and class neural network. The method can complete the detection of commutator surface defects through the comparison of independent object feature values in good and non-good images. The test results show that the commutator surface defect detection method proposed in this study can effectively overcome the problem of light reflection from the metal surface or rotation of the object to be inspected during filming, and well solve the problem of object shrinkage caused by binarization of the image. And the accuracy rate is up to 99% with fast processing time.*
Keywords: Class neural network, Commutator surface defect detection, Binarization segmentation, Region of interest division

1. **Introduction.** Machine vision with its advantages of non-contact, high accuracy and high speed has been widely used and achieved excellent results in defect detection, dimensional measurement, object recognition and unmanned vehicles1. For example, Bhuvanesh and Ratnam designed a machine vision-based defect detection algorithm for wire frames [1], which obtains the feature values in the wire by image binarization, corrects the image offset or rotation by analyzing the mass center of gravity, and uses the corrected image to compare with the standard image for defect detection. Perng et al. studied a wafer appearance defect detection method based on machine vision technology, which uses 2D light irradiation to perform inter-tin ball center coordinate positioning and calculate its cumulative gray scale value to complete the determination of wafer defects [2, 3].

Sheng et al. [4] and Gibert et al. [5] proposed a thread defect detection algorithm based on machine vision technology. This algorithm uses the Canny algorithm to extract the edge features and edge point locations of thread images, and identifies thread appearance defects by calculating and fitting the crest and trough points of threads. Wang et al. [6]

proposed a computer vision-based method for steel surface defect detection. The method is based on morphological grayscale curve envelope, and the effective filtering of the noisy part of the transverse grayscale curve of steel surface images and the preservation of the defective part are achieved by regression smoothing, curve benchmarking and deviation calculation steps; and the suspected defective region in the complex background environment of steel is obtained by the threshold selection of the region of interest and the merging of the region of interest. The experimental results show that the morphological grayscale envelope of the region of interest extraction can reduce the noise interference more than other methods, and the accuracy can reach more than 95%. Although vision-based detection methods have made a great breakthrough in performance and efficiency compared to manual detection, the accuracy of detection still cannot meet the requirements of defect detection performance due to its limited feature extraction capability. Therefore, the application of deep learning techniques with automatic feature extraction capability to improve the performance of machine vision has become a new hot spot for research in this field, and many research results have been generated. For example, Li et al. [7] used deep convolutional neural networks to identify individual component defects of railway tracks with an accuracy of 93.35%. Li et al. [8] proposed a deep learning based defect detection method. The method uses a deep learning model to reconstruct the image relationship between defective samples and defect-free samples, and achieves defect detection by comparing between defect-free and defective images 6. Girshick et al. [9] proposed an iterable deep learning method for the overfitting problem of small data sets in deep learning for artifact detection, and the experimental results showed that the method can effectively improve the recognition rate and reduce the overfitting of data [10, 11]. Due to the problems of uneven surface illumination, low contrast between defects and non-defects, and high similarity between noise and subtle defects, the current surface defect detection technology is still facing problems such as causing low recognition accuracy and slow detection speed. In particular, similar to workpieces with large commutator surfaces, high reflectivity, and complex appearance structures, it is extremely easy to have difficult classification, false detection, and missed detection due to the requirement to have an accurate match between the image to be inspected and the template image, and accurate detection requires the development of an automatic optical inspection (AOI) system with deep learning capabilities. Liu et al. [12] proposed a point cloud-based commutator surface defect detection method for commutator surfaces with large surfaces and high reflectivity, and the disadvantages of traditional manual inspection such as low accuracy, time consuming and missed misdetection, which can obtain get more accurate defect labeling and classification effects by comparing point cloud alignment-based and workpiece feature-based defect detection methods [13, 14]. It provides a new research direction for commutator defect detection method.

2. **Research Methodology.** In this study, the process of commutator surface defect detection can be divided into three major parts, firstly, the image pre-processing part, where the independent object features (such as perimeter, area, etc.) connected to the normal image are stored in advance, and the acquired image is divided into different regions for detection in the way of ROI (Region Of Interest) to save the steps of image correction. Secondly, the object independence and volume standardization of the image to be measured are carried out, and the object feature values in the image to be measured are calculated at the same time after the object independence of the whole image to be measured is completed; Finally, the determination of the commutator surface defects is carried out by using a neural network-like comparison of the object feature values. The detailed flow chart is shown in Figure 1.

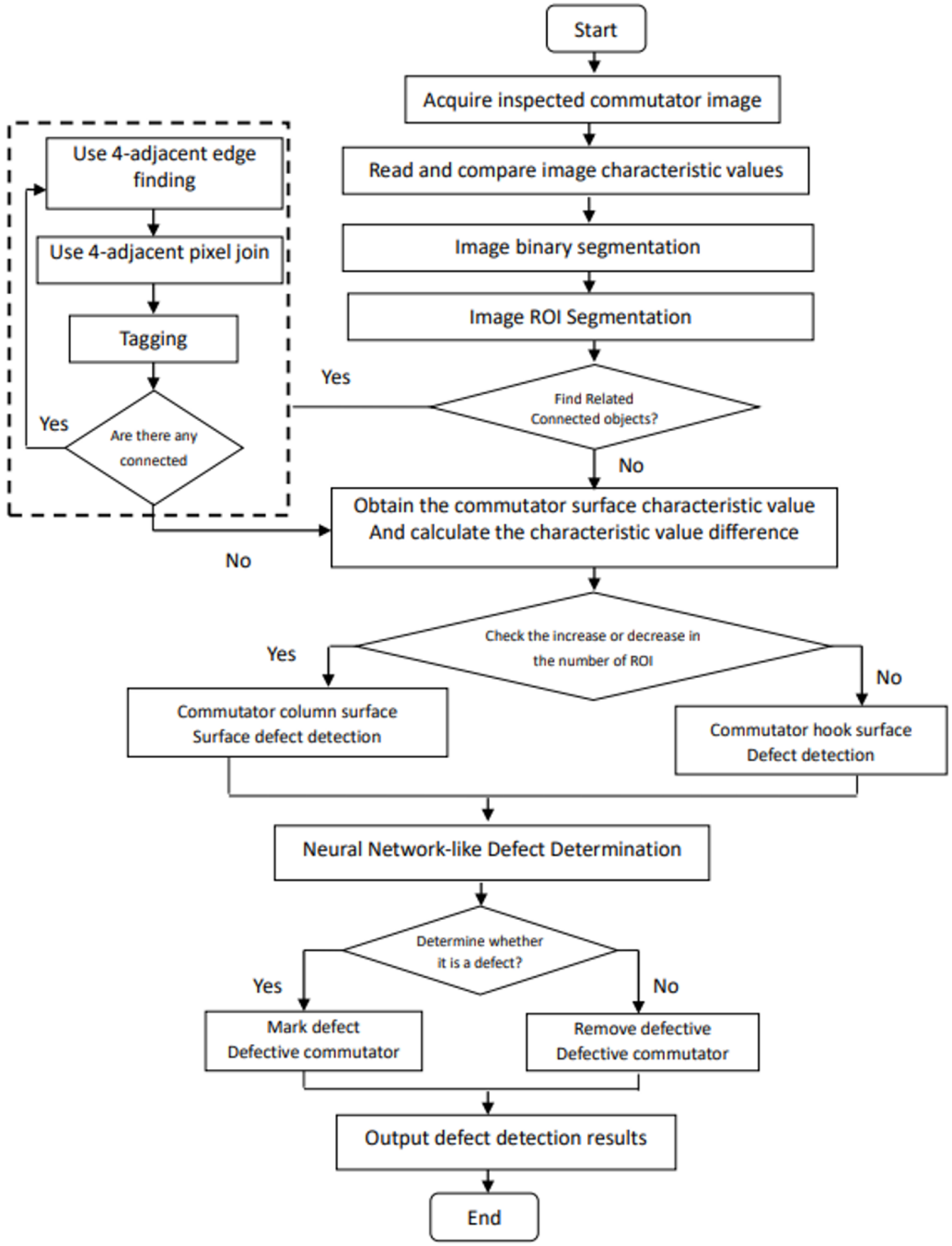

Figure 1. Flow chart of commutator surface defect detection based on class neural network

2.1. **Defect type and identification mode.** This study for commutator surface defect detection as shown in Figure 2, including column surface slot defects (including: bruising, under groove, scratching bright, black spot, dirty surface, tin color, outer circle bruising, outer circle slag, outer circle embossing, outer circle burr, outer circle thread, dirty surface, oil, outer diameter not round, outer circle scratch, outer circle brush damage, outer circle tail gap, outer circle tail crush, slot edge burr, slot bruising, hook end bruising defects) and hook surface defects (including reinforcement breakage, bakelite breakage, bakelite cracking, hook top burr, hook top cracking, hook root cracking, black skin, scraping,

chipping, bruising, hook tip damage, hook delamination, and under-hook oiling); As the connected objects are different in area and appearance. For the efficiency of image inspection, we record the feature values of the objects in the normal image in the developed program in advance, and then simply obtain the feature values of each object in the test image for comparison to know the inspection results. Depending on the type of defects two surface defect detection algorithms will be used in this study.

(1) Figure 2 (a) and (b) are both an independent object, on the surface defects are simply a reduction or increase in the area of the object, such defects will only need to obtain the area, perimeter and circularity of the independent object on the image to be tested and feature values, compared with the area of the object on the normal image, the defect can be discriminated.

(2) Figure 2 (c) defects caused by fracture, so that the original single independent object into two independent objects, this type of defects to be measured in the image processing, the number of independent objects after the area division and the number of objects in the normal image area for comparison, the use of class neural network for commutator surface defect determination, the original number of defective objects feature value combined calculation, together with other independent objects in the class The neural network performs the determination of good and defective products.

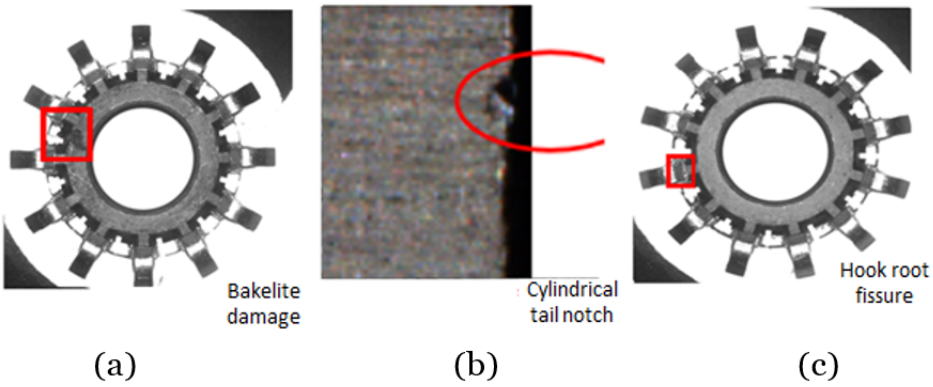

Figure 2. Typical commutator surface defect example

2.2. **Area division of the image to be measured.** In this study, the complete image is divided into several different blocks, and the division process is divided into two steps: general division and accurate division. First, the general division is performed to determine whether the object is included in the divided area, and the following settings are made in the general division.

(1) An independent object in an image to be measured, no matter how to offset or rotate, can't texceed the range of the shooting resolution 1024×1024 pixels, the actual situation is shown in Figure 3.

(2) The offset of the object should not exceed 21 pixels up, 5 pixels left, 7 pixels down, and 11 pixels right, and the rotation offset of the object should not exceed 2 degrees counterclockwise or clockwise to ensure that all objects are not outside the range of the whole image. Under this setting, the generalized division can perform its correct division function, and the generalized division is given at the early stage of design. The range of generalized division is assumed to be (,) as the coordinates of the upper left corner x_0 of y_0 the rectangular shape and (,) as the coordinates of the $x_1 lower\ y_1 right$ corner of the rectangular shape, by which the coordinates of these two points can constitute the range of generalized division, and the range is shown in Table 1.

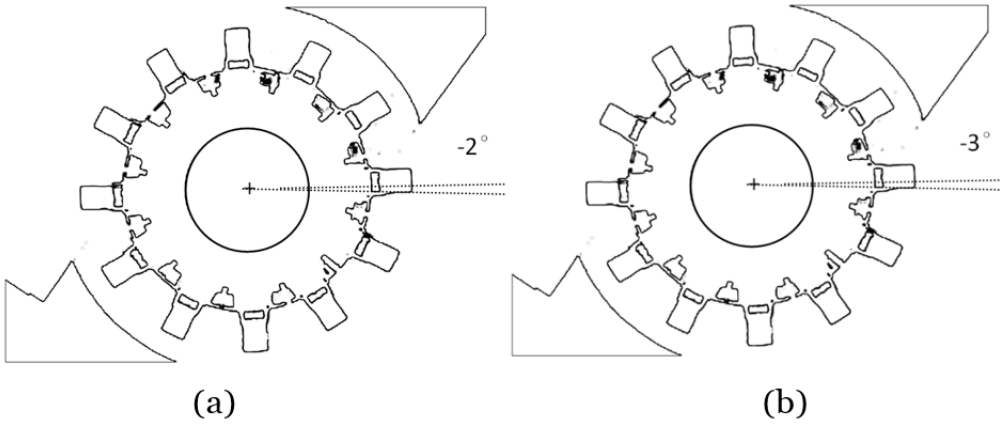

Figure 3. Image rotation offset allowed and out of range diagram (a)Rotation within the allowed range (-2°), (b) Rotation outside the range (-3°)

Table 1. Scoping for generalized classification.

	Region Of Interest (ROI)										
	01	02	03	04	05	06	07	08	09	10	11
$\mathbf{x_0}$	0	0	270	270	270	230	230	235	235	910	0
$\mathbf{y_0}$	0	120	110	220	335	465	560	648	735	150	840
$\mathbf{x_1}$	1024	170	830	820	825	860	865	860	865	1024	1024
$\mathbf{y_1}$	110	840	217	330	450	650	735	735	830	805	1024

2.3. **Object Independence.** In this paper, the accuracy search is performed by automatic judgment, and the judgment method is to search the object pixel coordinate values of the edges of all independent objects in the area of generalized division and correct the range of generalized division, and the actual difference between its generalized and accuracy division is shown in Figure 4. After the commutator image is divided by generalization and accuracy division, only the direction of the control system searching objects can be achieved to control the order of independent object volume labeling. At the same time, only the objects within the region of interest need to be processed, which can also improve the execution efficiency of subsequent image processing.

The content of the independent operation includes: object edge seeking, object filling, giving labels, continuous recursion for object independent, label number reordering (ascending order), complete object independent after the completion of the complete image. Find edges are independent for the whole object and different find edges can be used to obtain the boundary of the commutator surface defect type.

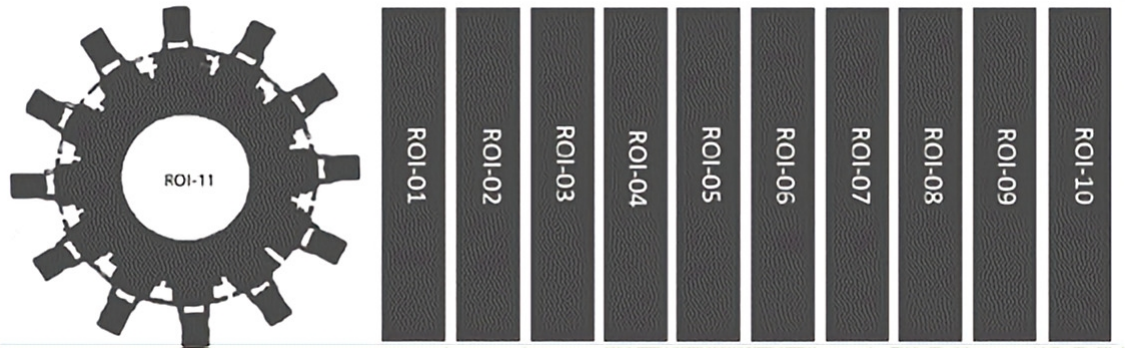

Figure 4. Schematic diagram of commutator image area division

Table 2. Table of directions for the 11 partitioned regions in Figure 6 applicable to object independentization.

Category	Area of interest	Direction	Applicable
1	01, 02, 03, 04, 05, 06, 07, 08, 09, 10	Scanning from top to bottom	Vertical distribution
2	ROI-11	Scan from left to right	Horizontal distribution

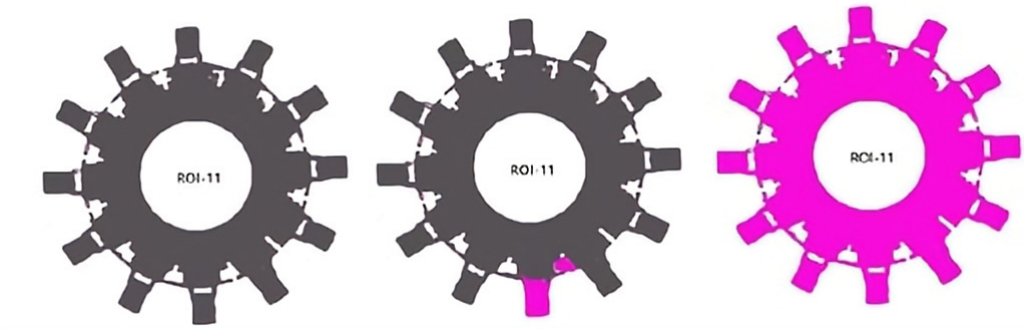

Figure 5. Schematic diagram of the individuation process of ROI-11 objects

Since the object of this study has a clear contrast between the object and the background, the binarization is beneficial, so the boundaries can be clearly separated, and the boundaries can be obtained quickly and correctly by using the general edge-seeking method. We determine whether there are 8 neighboring pixels of $f(x, y)$ any object-hair pixel point belonging to the background-hair pixel, and if there are, it will be $f_i(x, y)$ judged as a boundary point. According to the aforementioned method, the first partitioned area ROI-01 is scanned and operated to separate the connected objects, and it is clear that the left most to the right connected objects from ROI-01 are scanned and operated in order from top to bottom and from left to right. Then, we repeatedly repeat ROI-2 to ROI-11, until all the connected objects of the whole graph are independent. The scanning connected objects algorithm is a volume labeling scanning method used for the first scanning category in Table 2. If we assume that the length and $h_i \times w_i$ width of ROI-i are pixels, and the starting point of $f(x, y)$ the upper left corner is, the implementation of the algorithm is shown below.

Procedure Connected components
For x to $x + h_i$ do
For y to $y + w_i$ do
If $f_i(x, y)$ belongs to an object then
Perform the edge detection procedure.
Assign a label code to $f_i(x, y)$
End If
End For
End For
End Procedure Connected components

Classes 2 to 4 in Table 2 are scanned in a similar manner to Class 1, except that the scanning direction is different. The object volume labeling is to divide the object into 11 blocks, and to process the object independently in different directions. That is, using different scanning directions, edge finding is performed first, and then 4-adjacent concatenation is performed, and only after completion can labeling be performed.

2.4. **Acquired eigenvalues and eigenvalue deviation rate.** As there are three types of commutator surface defects in this study, the identification methods are as described in Section 3.1. In terms of object feature value acquisition, this study discriminates surface defects by calculating the area, parameter and circularity of the independent object, while the center of gravity feature value is mainly used for the positioning of the independent object, and these three feature values and their deviation rates are described below.

(1) Using the area and perimeter can simultaneously achieve the purpose of object surface defects detection, the area is calculated as the number of pixels in the whole image of the number of scanned objects, while the perimeter is calculated and the number of pixels adjacent to the background, when the difference between the normal image and the image to be measured is greater than the threshold value set, that is, defects, calculated as shown in the Equation (1), (2). Where mand nis the height and width of the detected image. If $f_i(x,y) \in k$,then area is

$$a_k = \sum_{y=0}^{m-1} \sum_{x=0}^{n-1} f_i(x,y) \tag{1}$$

If one of the 4-neighbors of object pixel $f_i(x,y)$ belongs to background, then perimeter is

$$a_k = \sum_{y=0}^{m-1} \sum_{x=0}^{n-1} f_i(x,y) \tag{2}$$

(2) The center of gravity is the use of 11 regions and the control of scanning direction to achieve the purpose of volume coding. However, it is found that this approach alone is not enough. The order of object coding often changes due to image rotation or displacement, especially in the area where two objects are close to each other, such as ROI-02 and ROI-11 as shown in Figure 7. Therefore, after each object is independent and its center of gravity is calculated for positioning, each ROI will be scanned again in the direction of the sequence Table2 to reset the order of independent objects, and the center of gravity of the object scanned first will be given to the previous object coding, after experimental confirmation, each independent object can be correctly sorted under the image partial shift and rotation, and its center of gravity is calculated as shown in Equation (3).

If object $f_i(x,y)$, then the mass center is

$$M_k(x,y) = \left(\frac{1}{a_k} \sum_{i=0}^{n-1} x_i \frac{1}{a_k} \sum_{j=0}^{m-1} y_i \right) \tag{3}$$

(3) Roundness

In order to know the proportional relationship between area and perimeter, the circularity can be used to represent, so together with the area and perimeter as the input layer of the class neural network for the recognition of commutator surface defects, which is defined as shown in Equation (4).

$$Circularity\ C_k = \frac{p_k^2}{4\pi \bullet \alpha_k} \tag{4}$$

(4) Deviation rate of eigenvalue

In order to highlight the commutator surface defects, the image to be measured is subtracted from the pre-stored defect-free image feature values, and the percentage of the subtracted feature values to the normal image feature values is calculated as the basis for identification, including the three geometric feature values of area, perimeter and

circularity, which is shown in Equation (5).

$$Value\ deviation\ rate\% = \frac{|Image\ Value\ to\ be\ tested\ -\ Normal\ image\ Value|}{Normal\ image\ Value} \times \% \quad (5)$$

2.5. **Selection of normal images.** When the image to be measured due to binarization caused by the case of shrinkage and expansion, often use the morphological expansion and erosion operations to deal with the image to be measured. Take commutator surface defect as an example, when the commutator surface reflection exists, the erosion operation is used to process the image to be measured, which will easily cause defect misjudgment, as shown in Figure 6. Similarly, if there are no defects on independent objects and they are close to each other, processing the image to be measured by the expansion operation often causes the connection of two independent objects, which easily increases the uncertainty in image processing and misjudgment in defect detection. Based on the abnormal conditions caused by object erosion and expansion, this study proposes that the normal image should be selected based on the total area of all objects in the whole image to be measured, so that it can be used as a reference basis for obtaining the feature values of the image to be measured. The law of selection is shown in Equation (6).

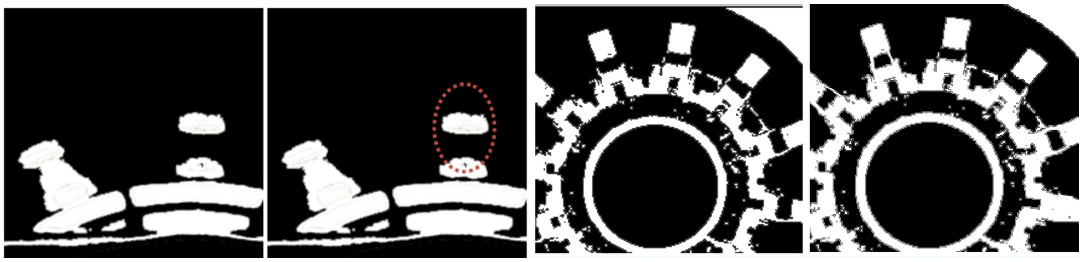

Figure 6. Image morphology erosion and swelling results

2.6. **Surface defect identification using back-passage class neural network.** The discrimination of commutator surface defects is performed using Back-Propagation Network (BPN) [15], a class of neural networks, which is a supervised learning network, and the network architecture set in this study is shown in Figure 7. The area (ak), perimeter (pk), and circularity (Ck) deviation rates obtained from the independent objects are considered as the input nodes of the neural network to identify defects or good products, so three input nodes () and one xoutput node () are used yas the main architecture.

Compute the total areas of objets in the image to be measured, and select the standard image for comparison according to the above Equation.

Compute the total $\sum_{k=0}^{n} a_i$ areas of objcets in a test image;

$$if \begin{cases} \sum_{i=1}^{k} a_i \geq \frac{N1+N2}{2} & ;\ then\ use\ 1\ image. \\ \frac{N1+N2}{2} > \sum_{i=1}^{k} a_i \geq \frac{N2+N3}{2}; & then\ use\ 2\ image. \\ \frac{N3+N3}{2} > \sum_{i=1}^{k} a_i \geq \frac{N3+N4}{2}; & then\ use\ 3\ image. \\ \sum_{i=1}^{k} a_i < \frac{N3+N4}{2} & ;\ then\ use\ 4\ image. \end{cases} \quad (6)$$

The number Hof nodes in the hidden layer () was set using the rule of thumb suggested in the literature, as shown in Equation (7), and in the subsequent experiments, the number

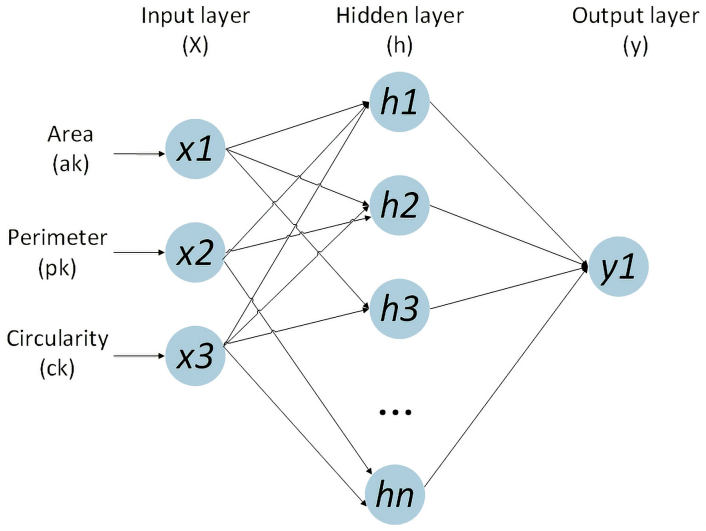

Figure 7. Architecture of the inverse transfer class neural network

of nodes in the hidden layer was p fine-tuned and the weight matrix was set in a uniformly distributed manner with random W_hrandom W_ynumbers.

$$\frac{Number\ of\ input\ layer\ nodes + Number\ of\ output\ layer\ nodes}{2} = Number\ of\ hidden\ layer\ nodes \tag{7}$$

The network undergoes iterative training process, then the root mean square of error is used to measure the degree of network convergence during the training process, as shown in Equation (8), and learning can be stopped if the network has reached the convergence target.

$$R_{MSE} = \sqrt{\frac{\sum_{P}^{M}\sum_{j}^{N}\left(T_j^p - Y_j^P\right)^2}{M \bullet N}} \tag{8}$$

This study uses inverse transfer neural network for commutator surface defect recognition, and the BPN has high learning accuracy and can handle complex sample recognition problems with highly nonlinear function synthesis problems. The trained BPN has a very fast recall speed, which is suitable for real-time detection of online commutator surface defects. To verify the practicality of the above method, the following details the experimental procedure and result analysis [16].

3. **Experiment and Result Analysis.** This study was conducted in Microsoft Win10 operating environment for simulation experiments. The commutator surface defect detection system was developed using C++ programming language, and MATLAB 7.0 was used for network parameter training.

3.1. **Detection requirements.** When the commutator image of this study is taken, often due to the interference of shooting parameter adjustment or light reflection factors, the binarization process of the photographed image may cause the expansion or erosion of the object in the image due to the selection of different threshold values, and if the surface defects are detected by comparing with the normal image, it is easy to make a false judgment. In this study, we prepare standard images that can accommodate both the expansion and contraction of images with the maximum and minimum image cutting threshold values.

1). Sample characteristics and the influence of external factors

The commutator image will be affected by the selection of different threshold values after binarization, resulting in different degrees of expansion and contraction of the connected independent objects in the image; in addition, the shaking of the commutator image during the shooting process, metal surface reflection and other factors, there will be a shift or rotation of the phenomenon must be overcome.

2). Processing time of the detection system

Since the automated inspection equipment needs to be paired with production equipment for online real-time inspection, its image processing speed must be completed within a certain period of time, from image acquisition, pre-processing, image processing and defect identification to result output, the general processing time must be completed within 5 seconds, according to repeated experimental results show that the system from image acquisition to binarized image before about 2 seconds of time (image acquisition about 1 second, image pre-processing about 1 second). Therefore, the second half of the processing procedure of this system must be completed within 3 seconds for the detection of commutator surface defects.

3). Correct detection rate and error rate of defect inspection

In this study, the defect detection performance is evaluated by using the general industry requirements for vision systems, i.e., the correct detection rate of defects must reach 90% or more, and the misjudgment rate of defects must be less than 10%.

3.2. **Benefit evaluation index.** This study uses statistical methods to measure the detection effectiveness of the defect detection system, as the experiments are conducted in batches of 64 test images and the number of correct and false detections are calculated, the evaluation indexes used are defined as shown in Equations (9) to (11).

$$\text{Defect detection rate}(1-\beta) = \frac{\text{Number of defects correctly detected}}{\text{total number of real defects}} \times 100\% \quad (9)$$

$$\text{Defect misjudgment rate}(\alpha) = \frac{\text{Number of defects misjudged in normal area}}{\text{Number of defects detected}} \times 100\% \quad (10)$$

$$\text{Correct classification rate (CR)} = \frac{\text{Number of correct identification}}{\text{Number of samples}} \times 100\% \quad (11)$$

3.3. **Detection parameter setting.** The inverted transfer class neural network is a supervised learning network, and it is necessary to train its network parameters before conducting the determination of commutator surface defects and good products. 53 images of normal images and 53 test images are used as training images in this study. The parameters of the class neural network are set with $a, 1-\beta$, CR (the number of times the network is repeatedly trained)and the network convergence error as response variables for analysis. In order to understand the number of convergence and convergence error of the network, the tolerance error was set to and the number 10^{-20} of network training for 10^4 network training when performing network training. The factors with high significance were then used in a multilevel factorial design to find the best parameter settings. Table 3 shows the parameters and level settings of the fixed and control factors adjusted during the experimental phase.

1). 1st experimental design analysis

The main purpose of the first experimental design was to find out the factors with high significance, and some of the factors were explored in a two-level factorial design, and the detection efficiency of the network constructed by different training functions was compared. The experimental data and results are shown in Table 4, while Table 5 shows

Table 3. Factor settings of the experimental design.

Factor settings	Factor name		Setting range	Horizontal design
Control factor	A	Number of hidden layer nodes	1 to 5	Two levels: 1 (low A_1 level,), 5 (high level,) A_2
				Multi-level: 1, 2, 3, 4, 5
	B	Learning rate	0.01 ∼ 0.9	Two levels: 0.01 (low B_1 level,), 0.5 (high level,) B_2
				Multiple levels: 0.01, 0.05, 0.1, 0.3, 0.5
	C	Training function	LM	Level $C_1$1() error back propagation neural network algorithm
			GD	Level $C_2$1() Gradient Descent Backpropagation Algorithm
			GDA	Level $C_3$1() momentum back propagation gradient descent method
			GDM	Level $C_4$1() momentum gradient descent method
Fixed factor	Number of output nodes		1	When the output value is 1, it is judged to be defective, while when the output value is 0, it is judged to be defect-free.
	Number of hidden layer network layers		1	Since the input node is 3 and the output layer node is 1, is not a complex problem, the defective commutator is identified with layer1.

the average detection results of each factor level. The results of the first experimental design are analyzed as follows.

From the analysis results in Table 5, we know that when using the LM training function for network training, although there will be some defects missed, but there will be a higher detection rate for defect detection, so the subsequent experiments, then use LM as the training function for the network.

Table 4. Experimental data of the first experimental design.

Parameters	Control variables		Reaction variables				
	A: Hidden layer node	B: Learning speed	Number of training sessions	Convergence error	a (%)	$(1-\beta\%)$	CR (%)
Combinations	1	0.01	LM	938	0	1.00	98.02
2	5	0.01	LM	10000	2.2E-07	1.67	97.36
3	1	0.5	LM	1056	0	1.00	98.02
4	5	0.5	LM	10000	0.0027	0.66	99.01
5	1	0.01	GD	10000	0.0157	0.00	83.17
6	5	0.01	GD	10000	0.0155	0.00	93.73
7	1	0.5	GD	10000	0.0267	0.00	80.53
8	5	0.5	GD	10000	0.0143	0.00	96.37
9	1	0.01	GDM	10000	0.0711	0.00	26.07
10	5	0.01	GDM	10000	0.0148	0.00	95.05
11	1	0.5	GDM	10000	0.0107	0.00	96.37
12	5	0.5	GDM	10000	0.0118	0.00	95.05
13	1	0.01	GDA	10000	0.0999	0.00	84.16
14	5	0.01	GDA	10000	0.0103	0.00	94.72
15	1	0.5	GDA	10000	1.3E-02	0.00	96.70
16	5	0.5	GDA	10000	0.0100	0.00	96.04

Table 5. Mean test results for each factor level.

Control factor water Level Average effect		Number of training	Convergence error	(a %)	$(1-\beta\ \%)$	CR (%)
A:Number of hidden layer nodes	1	7749	0.030	0.25	82.88	99.56
	5	10000	0.010	0.29	95.92	99.89
B:Learning rate	0.01	8867	0.028	0.33	84.03	99.58
	0.5	8882	0.011	0.21	94.76	99.86
C:Training function	LM	5499	0.001	1.08	98.10	99.92
	GD	10000	0.018	0.00	88.45	99.70
	GDM	10000	0.027	0.00	78.14	99.44
	GDA	10000	0.033	0.00	92.90	99.82

(3) When the number of nodes in the hidden layer is too small, the phenomenon of too little or over-training will occur. In order to get the optimal setting parameters, the 5^2 2nd experimental design is carried out in this paper with factors.

2). 2nd experimental design analysis: 5^2 factorial design

After obtaining some of the parameter settings, two important parameters affecting network recognition were then designed at a finer level to find the ideal network parameter settings, distinguishing the number of hidden layer nodes as 1, 2, 3, 4, 5 and learning rates as 0.01, 0.05, 0.1, 0.3, 0.5, respectively, and executing the inverse transfer class neural network to discriminate the defective products to explore the ideal detection results.

According to the rule of setting the network parameters, the learning rate is set to 0.1 in order to keep the appropriate learning rate, which will have better results for defective product identification. The results were not significant according to the number of training sessions and convergence errors, as shown in Table 6, item 3, 8, 13, 18, and 23 for the experimental parameter combinations. Finally, the results of the two experimental designs were integrated, and the network parameters were set according to Table 6 to obtain good detection results, i.e., 99% defect detection rate and 0.66% misjudgment rate, 99.96% overall correct judgment rate, and 2.7 seconds required detection time.

Table 6. Factorial design results of 5^2 the second experimental design.

Parameter Combination	Control variables		Reaction variables				
	A:Hidden layer node	B: Learning speed	Training times	Convergence error	a	$1-\beta$	CR
1	1	0.01	1038	0	1.00	98.02	99.92
2	2	0.01	10000	0.00201	1.95	99.67	99.94
*3	3	0.01	10000	0.001809	0.66	99.01	99.96 *
4	4	0.01	10000	0.000696	5.14	97.36	99.80
5	5	0.01	10000	4.97E-05	5.03	99.67	99.86
6	1	0.05	1298	0	1.00	98.02	99.92
7	2	0.05	3538	0	0.67	98.35	99.94
*8	3	0.05	10000	0.001809	0.66	99.01	99.96 *
9	4	0.05	10000	0.001113	1.32	98.35	99.92
10	5	0.05	10000	2.62E-09	4.47	98.68	99.85
11	1	0.1	931	0	1.00	98.02	99.92
12	2	0.1	418	0	1.00	98.02	99.92
*13	3	0.1	10000	0.001809	0.66	99.01	99.96 *
14	4	0.1	10000	0.000728	5.64	99.34	99.83
15	5	0.1	10000	8.36E-12	3.87	98.35	99.86
16	1	0.3	1355	0	1.00	98.02	99.92
17	2	0.3	6678	0	0.67	98.35	99.94
*18	3	0.3	10000	0.001809	0.66	99.01	99.96*
19	4	0.3	10000	0.00109	1.00	97.69	99.92
20	5	0.3	10000	1.57E-05	4.72	100.0	99.87
21	1	0.5	1159	0	1.00	98.02	99.92
22	2	0.5	3674	0	0.67	98.35	99.94
*23	3	0.5	10000	0.001809	0.66	99.01	99.96 *
24	4	0.5	10000	1.27E-05	5.03	99.67	99.86
25	5	0.5	10000	0.00287	0.98	99.67	99.97

Table 7. Optimal network parameters and their detection results.

Optimal Parameter Setting	Training results			Detection results			
	Number of hidden layer nodes	Network training speed	Network training function	a	$1-\beta$	CR	Time(s)
	3	0.1	LM	0.66 %	99.01 %	99.96 %	2.7 s

Table 8. Deviation rate of defective misclassified commutators and their characteristic .

No. (Position)	Image_1 (Position:139)	Image_2 (Image:98)	Image_3 (Image:171)	Image_4 (Image:73)	Image_5 (position:83)
Images					
Three Eigenvalue	a139 = 2.19%	a98= 1.79%	a171=1.83%	a73=1.62%	a83 = 1.54%
	p139 = 6.25%	p98 = 16.48%	p171 = 0.86%	p73 = 3.42%	p83 = 1.64%
	c139 = 10.14%	c98 = 38.16%	c171 = 0.12%	c73 = 8.71%	c83 = 1.73%
No. (Position)	Image_1 (Position:139)	Image_2 (Image:98)	Image_3 (Image:171)	Image_4 (Image:73)	Image_5 (position:83)
Images					
Three Eigenvalue	a126 = 1.21%	a118 = 1.35%	a134 = 1.21%	a171 = 1.83%	a44 = 1.72%
	p126 = 0.00%	p118 = 0.00%	p134 = 0.00%	p171 = 0.86%	p44 = 1.54%
	c126 = 1.23%	c118 = 1.37%	c134 = 1.23%	c171 = 0.12%	c44 = 1.36%

3.4. **Analysis of Image Conversion Benefits.** The image of cylindrical commutator inspection may not be processed properly due to pose shift or rotation, so image correction is required for component shift and rotation before general image processing. In this study, the proposed method can detect surface defects without image correction. Therefore,

we will compare whether there is a significant difference between these two methods in terms of defect detection benefits, and evaluate them using three metrics: correct defect detection rate, false positive rate, and defect detection time. During the experiment, 53 images containing rotation and offset were used for testing with images affected by image binarization, and the comparison results are shown in Table 9. That is, under the same detection method, the results show that there is no significant difference in the correct detection rate and error detection rate between the proposed method and the method with image correction. In terms of the average processing time, the average processing time in this study was about 0.708 seconds, which not only eliminated the image correction process, but also reduced the time by 24%.

Table 9. Benefit analysis results of image processing with and without correction.

Item	a	$1-\beta$	Time (s)
Surface defect detection system without image correction	0.66 %	99.01 %	2.72 s
Surface defect detection system with image correction	0.66 %	99.01 %	3.43 s

4. **Conclusion.** In this study, we propose to use spatial domain image processing technology and neural network for the detection of surface defects in a commutator. By obtaining the feature values of the independent object in the image to be measured and comparing them with the normal image, and then using the backward transfer neural network to discriminate the defects, we can complete the detection of surface defects in the commutator. This method can not only overcome the problem of light reflection or cylinder rotation due to the metal surface when shooting, but also solve the problem of object shrinkage caused by the image after binarization. The experimental results show that the detection rate of commutator surface defects of the proposed method is up to 99%, and it has a fast processing time (2.7 seconds for a 1024×1024 pixel image). It is worth to be promoted in industrial inspection to improve the product surface defect detection rate. Since the detection benefit assessment of this study, using a only, $1-\beta$ and CR and other multiple quality assessment indexes, fails to fully reflect the goal of optimizing multi-type and multi-quality detection parameters, more effective and fast product defect detection algorithms should be further explored in the future for the multi-objective and multi-quality needs of online product defect detection to achieve more desirable detection results.

Acknowledgements. Guangdong University Student Science and Technology Innovation Cultivation Special Fund Grant (pdjh2021b0945); Dongguan Science and Technology of Social Development Program: 20211800904452; Dongguan Sci-tech Commissoner Program. (Grants NO.20201800500432); 2022 Innovation Team Project of Colleges and Universities of Guangdong Province (Project No.: 2022KCXTD063, Project Name: Intelligent equipment innovation team based on machine vision).

REFERENCES

[1] A. Bhuvanesh, and M.-M. Ratnam, "Automatic detection of stamping defects in lead frames using machine vision: overcoming translational and rotational misalignment," *International Journal of Advanced Manufacturing Technology*, vol. 32, no. 12, pp. 1201-1210, 2007.

[2] D.-B. Perng, C.-C. Chou, and S.-M. Lee, "Design and development of a new machine vision wire bonding inspection system," *International Journal of Advanced Manufacturing Technology*, vol. 34, no. 3, pp. 323-334, 2007.

[3] B.-H. Shi, and Y.-H. Wei, "A thread defect detection method based on machine vision," *Journal of Three Gorges University (NATURAL SCIENCE EDITION)*, vol. 2, pp. 64-66, 2015.

[4] G.-F. Sheng, W.-X. Lei, F. Deng, and R.Q. Yuan, "Region of interest extraction method for steel surface defect image," *Mechanical Design and Manufacturing*, vol. 1, pp. 152-155, 2017.
[5] X. Gibert, V.-M. Patel, and R. Chellappa, "Deep multitask learning for railway track inspection," *IEEE Transactions on Intelligent Transportation Systems*, vol. 18, no. 1, pp. 153-159, 2017.
[6] X.-B. Wang, J. Li, and M.-H. Yao, "Surface defect detection method of solar cell based on deep learning," *Pattern Recognition and Artificial Intelligence*, vol. 6, pp. 517-523, 2014.
[7] T.-F. Li, and Y.-B. Qin, "Defect detection based on iterative deep learning," *Computer and Digital Engineering*, vol. 45, no. 6, pp. 1133-1137, 2017.
[8] Y.-M. Li, X.-B. Duan, and S.-L. Ma, "Commutator surface defect detection method based on point cloud. Computer and Modernization," vol. 10, pp. 101-107, 2019.
[9] R. Girshick, J. Donahue, T. Darrell, and J. Malik, "Rich feature hierarchies for accurate object detection and semantic segmentation," *IEEE Conference on Computer Vision and Pattern Recognition*, pp. 741-749, 2014.
[10] R. Girshick, "Fast R-CNN," *IEEE International Conference on Computer Vision*, pp. 1321-1329, 2015.
[11] S. Ren, K. He, R. Girshick, and J. Sun, "Faster R-CNN: Towards real-time object detection with region proposal networks," *Advances in Neural Information Processing Systems*, vol. 32, pp. 601-69, 2015.
[12] W.-D. Liu, D. Erhan, C. Szegedy, S. Reed, and A.C. Berg, "SSD: Single Shot Multi-Box Detector," *European Conference on Computer Vision (ECCV)*, pp. 1033-1038, 2016.
[13] J. Redmon, and A. Farhadi, "YOLO9000: Better, Faster, Stronger," *Conference on Computer Vision and Pattern Recognition (CVPR)*, pp. 689-703, 2017.
[14] A. Soltoggio, "Born to learn: The inspiration, progress, and future of evolved plastic artificial neural networks," *Neural Networks: the official journal of the International Neural Network Society*, vol. 108, pp. 48-67, 2018.
[15] M. Volodymyr, K. Koray, and S. David, "Human-level control through deep reinforcement learning," *Nature*, vol. 518, no. 7540, pp. 529-33, 2015.
[16] R.-A. Amjad, B.-C. Geiger, "Learning Representations for Neural Network-Based Classification Using the Information Bottleneck Principle," *IEEE Transactions on Pattern Analysis & Machine Intelligence*, pp. 205-2122, 2018.
[17] A.-G. Álvaro, J.-A. álvarez-García, and L.-M. Soria-Morillo, "Evaluation of Deep Neural Networks for traffic sign detection systems," *Neurocomputing*, vol. 316, no. 17, pp. 332-344, 2018.